External forcing of spiral waves

Vladimir S. Zykov,[a] Oliver Steinbock,[b] and Stefan C. Müller
Max-Planck-Institut für Molekulare Physiologie, Rheinlanddamm 201, D-44139 Dortmund, Germany

(Received 12 April 1994; accepted for publication 12 July 1994)

The effect of an external rhythm on rotating spiral waves in excitable media is investigated. Parameters of the unperturbed medium were chosen, such that the organizing spiral tip describes meandering (hypocyclic) trajectories, which are the most general shape for the experimentally observed systems. Periodical modulation of excitability in a model of the Belousov–Zhabotinsky (BZ) reaction forces meandering spiral tips to describe trajectories that are not found at corresponding stationary conditions. For different modulation periods, two types of resonance drift, phase-locked tip motion, a spectrum of hypocyclic trajectories, and complex multifrequency patterns were computed. The computational results are complemented by experimental data obtained for periodically changing illumination of the photosensitive BZ reaction. The observed drastic deformation of the tip trajectory is considered as an efficient means to study and to control wave processes in excitable media.

I. INTRODUCTION

Spiral waves rotating in excitable media belong to the basic spatiotemporal patterns in nonequilibrium systems. They are observed in many biological media, such as cardiac tissue,[1,2] chicken retina,[3] the cellular slime mold *Dictyostelium discoideum*,[4] or in the cytoplasm of Xenopus oocytes.[5] They exist in distributed physicochemical systems, for instance, in the Belousov–Zhabotinsky (BZ) solution[6,7] and on platinum surfaces[8] used to catalyze the oxidation of carbon monoxide.

An excitable medium can be considered as a network of nonlinear oscillators coupled by diffusion. A spiral wave is the result of the self-organization of a large number of such active elements due to their local interaction. The appearance of a spiral wave creates a specific source of nonlinear oscillations in an active medium that contains both temporal and spatial features in close interplay. The spatiotemporal characteristics of the spiral wave is determined by the properties of the medium, and, if the size of the medium is sufficiently large, do not depend on the boundary conditions. Such spirals can rotate rigidly around a fixed circular core.[9] But, for another state of the medium, this core drifts in space, which leads to a compound rotation,[10–12] or even to irregular motion,[13,14] of the spiral tip. Thus, the spiral wave exhibits quite nontrivial dynamic properties, even for the familiar case of a stationary excitable medium.

All realistic media are embedded in some environment and thus undergo external forces and fields. Under this aspect it becomes important to investigate the evolution of spiral waves under nonstationary conditions. Nonstationary regimes can also be considered as an effective means to control the spiral wave, for example, to move the core of the spiral wave through the medium.[15–17]

In this paper we study the effect of periodic variations of the medium parameters on the dynamics of the spiral waves. To this end we focus on the investigation of wave processes in the light-sensitive BZ reaction, which proves to be particularly suited for the external forcing.[18–20] We will use both computer simulations of the corresponding mathematical models and direct experimental observations of the spiral waves in the distributed BZ system. Thereby, we consider the BZ reaction as a laboratory case for the study of general properties of excitable media.

II. MATHEMATICAL MODEL

Many of the quantitative features of the BZ reaction can be explained by the kinetic description (Oregonator model) put forward by Field, Körörs, and Noyes[21] and Tyson.[22] This classical scheme includes the autocatalytic production of $HBrO_2$ with Ce(IV), used as a catalyst. The Br^- ions play the role of an inhibitor. In the light-sensitive BZ reaction, the catalyst Ce(IV) is replaced by the ruthenium–bipyridyl complex,[23,24] which promotes the autocatalytic production of the activator $HBrO_2$ only in its reduced and electronically unexcited state. Once the ruthenium complex is photochemically excited, it slowly catalyzes the production of the inhibitor bromide. Thus, externally applied illumination creates an additional source of inhibitor Br^-, and thus suppresses the excitability of the medium (for instance, it decreases the propagation velocity of excitation waves). The corresponding system of differential equations that describes these processes has the following form:[24]

$$\begin{aligned} \epsilon \frac{du}{dt} &= u - u^2 - w(u-q), \\ \frac{dv}{dt} &= u - v, \\ \epsilon' \frac{dw}{dt} &= fv - w(u+q) + \phi, \end{aligned} \tag{1}$$

where the variables u, v, and w describe the evolution of the $HBrO_2$, catalyst and bromide concentrations, respectively. The term ϕ represents the light-induced flow of Br^-. For

[a]Permanent address: Institute of Control Sciences, Moscow, Russia.
[b]Current address: Department of Chemistry, West Virginia University, P.O. Box 6045, Morgantown, West Virginia 26506.

 1054-1500/94/4(3)/509/10/$6.00

Tyson's "Lo" set of rate constants,[22] the order relation $\epsilon' \ll \epsilon \ll 1$ is valid. As a consequence, w can be assumed in quasiequilibrium, so that

$$w = \frac{fv + \phi}{u + q}. \tag{2}$$

Hence, one can reduce the system (1) to the modified two-variable Oregonator and include molecular diffusion:

$$\frac{\partial u}{\partial t} = \frac{1}{\epsilon}\left(u - u^2 - (fv + \phi)\frac{u - q}{u + q}\right) + \nabla^2 u,$$
$$\frac{\partial v}{\partial t} = u - v. \tag{3}$$

Here the Laplacian $\nabla^2 u$ describes the diffusion of the $HBrO_2$, while the catalyst is considered to be immobilized in the gel matrix. The term $\phi(t) = \phi_0 + A \sin(2\pi t/T_m)$ determines the periodical modulation of the additional Br^- flow with the modulation period T_m. The amplitude A of modulation has to be smaller than the constant flow ϕ_0, because the additional Br^- flow is always positive. The parameters $\epsilon = 0.05$ and $q = 0.002$ are fixed, and the actual values of the parameters f, A, and ϕ_0 are indicated in the following computations. These were performed by the explicit Euler method, with the five-point approximation of the Laplacian on a 380×380 array with a grid spacing $\Delta x = 0.1$ and time steps $\Delta t = 0.001$.

III. RIGID ROTATION AND RESONANCE

Rigid rotation is the simplest regime of spiral wave motion. Such a rotation occurs with a constant angular velocity around a ring-shaped core. The shape of the spiral wave does not change with time. A kinematical description of this rotation was elaborated, taking into account the velocity–curvature relation for the propagating front.[25,26]

The angular velocity and the size of the core should depend on the parameters of the medium. Hence, if the parameters of the medium suddenly jump to other values the trajectory of the spiral tip will approach with time a new circular path with a modified radius and a slightly displaced center. For the case of periodical variation of the parameters, such deviations of the center location should be accumulated in the course of time.

In Fig. 1, two examples of this type of tip trajectory are shown, computed for the model (3), with two different values of the frequency of external forcing. In both cases the tip moves along a cycloid, while, for the given parameters f and ϕ_0, the unperturbed spiral rotates rigidly. Hence the observed periodical changes of the curvature of the spiral tip trajectory are induced by small variations of the additional flow of bromide ions. The resulting curve includes rotation of the tip around a circle with radius r_0 as for the unperturbed case, and a motion of the center of the circular core on a large circle with radius R_c.

Such a phenomenon was described in the framework of the kinematical theory of wave processes in excitable media and is called resonance of the spiral wave.[26] It was shown in the limit of a small-amplitude A of the external forcing, that

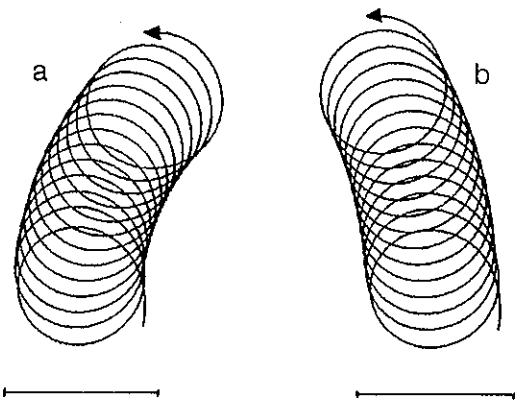

FIG. 1. Resonance drift of the spiral wave under an external modulation computed for model (3) with $f = 3.5$, $\phi_0 = 0.01$, and modulation amplitude $A = 0.0002$. Modulation period: (a) $T_m = 6.6$ and (b) $T_m = 6.7$. Scale bar: 10.0.

the radius R_c is inversely proportional to the difference between the autonomous frequency ω_r of the unperturbed spiral and the frequency of external force ω_m:

$$R_c \sim \frac{A}{\omega_r - \omega_m}. \tag{4}$$

Note that the sign of R_c differs for $\omega_m < \omega_r$ and for $\omega_m > \omega_r$ (see Fig. 1). For the case $\omega_m = \omega_r$ (full resonance), the core center moves along a straight line. The velocity of the core motion is proportional to the amplitude of external forcing A, and its direction depends on the initial phase of the spiral wave.

IV. CYCLOIDAL MOTION OF SPIRAL WAVES

Rigid rotation during which the spiral tip describes a circular trajectory is not the only possible regime of a spiral wave in a stationary excitable medium. In fact, for the experiments with the BZ reaction, cycloidal trajectories are observed more often[10–12, 14] than the rigid rotation. Simulations of spiral waves using different kinds of models for excitable systems[13,27–29] show that this is a common rule: cycloidal motion is a general case, while rigid rotation can be observed in the limiting cases of low excitability or small refractoriness of a medium.

Cycloidal regimes are observed in the model (3) for a wide range of parameter values f: $1.0 < f < 3.0$. In the following, we fix the value to $f = 2.0$ and study the role of external forcing imposed on the spiral wave behavior.

The three different cycloidal trajectories of the tip shown in Fig. 2 were computed for different values of the time-independent parameter ϕ_0 in (3) and for zero modulation amplitude. Such trajectories can be roughly approximated by hypocycloids,[10–12] including two general frequencies ω_1 and ω_2:

$$x = R_1 \cos \omega_1 t + R_2 \cos \omega_2 t,$$
$$y = R_1 \sin \omega_1 t - R_2 \sin \omega_2 t. \tag{5}$$

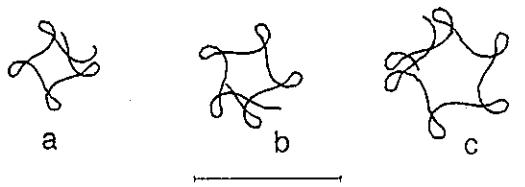

FIG. 2. Trajectories of the wave tip computed for model (3) with $f=2.0$ without external modulation ($A=0.0$) for three different values of the stationary external bromide flow ϕ_0: (a) $\phi_0=0.005$, (b) $\phi_0=0.01$, (c) $\phi_0=0.015$. Scale bar: 10.0.

The primary component of this compound motion can be interpreted as the tip rotation around a core with radius R_1, while the secondary component describes the motion of the core center around another circle with radius $R_2>R_1$. It is important that for a hypocycloid the secondary motion is clockwise, i.e., opposite to the counterclockwise primary rotation.

Let us now assume that the hypocycloid is closed after a time interval T and contains N lobes. In the simplest case the trajectory is closed after only one rotation period of the secondary motion and N is the general parameter of the trajectory. But in a more general case, it takes M rotations and the number n of lobes per one rotation of the secondary motion,

$$n=N/M, \tag{6}$$

is an important characteristic feature of the hypocycloid. This number determines, for instance, the ratio of the two frequencies ω_1/ω_2. Indeed, the frequency of the secondary motion is

$$\omega_2=2\pi M/T, \tag{7}$$

since M is the rotation number for the secondary motion. The rotation number for the primary motion is $N-M$, because this rotation has the opposite direction with respect to the secondary one. Therefore, the corresponding angular velocity is

$$\omega_1=2\pi(N-M)/T, \tag{8}$$

and the ratio of the two frequencies is given by the formula

$$\omega_1/\omega_2=n-1. \tag{9}$$

Due to the central symmetry of the hypocycloid, it is obvious that during the total period T the wave front passes N times through the central point. Therefore, the period of excitation T_0 that can be measured in the center of the hypocyclic trajectory is equal to

$$T_0=T_2/n, \tag{10}$$

where $T_2=T/M$ is the period of the secondary motion.

But one can also measure another period of excitation T_∞ in a point of the medium far away from the symmetry center. This value is inversely proportional to the number of rotations of the spiral wave completed during one total period T. As mentioned before, this number is $N-M$ because of the opposite directions of the primary and the secondary motion. Hence, the following expression is valid:

$$T_\infty=T_2/(n-1). \tag{11}$$

We emphasize that this value is equal to the period of the primary motion $T_1=2\pi/\omega_1$, as follows from (9) and (11):

$$T_\infty=T_1. \tag{12}$$

Thus, the period of excitation measured in the symmetry center of a hypocyclic trajectory T_0 is smaller than the period T_∞ measured far away from the center. Indeed, the period T_0 can be expressed from (10) and (11) as

$$T_0=T_\infty(n-1)/n. \tag{13}$$

Finally, there are five numbers that specify the temporal characteristics of the tip trajectory: T_0, T_∞, T_1, T_2, and n. The first two can be directly measured in the experiment, and the last three can be estimated by detailed analysis of the tip trajectory. Only two of these values are independent because they obey the three equations (11)–(13).

If the hypocycloidal trajectory is not closed, the quantity n is an irrational number. In this case, one needs to choose some approximation in terms of a rational number, and then the previous consideration is applicable.

V. PRIMARY AND SECONDARY RESONANCE

The resonance for a compound rotation should be more complicated than the resonance for a rigidly rotating spiral wave, since the compound rotation is characterized at least by two different frequencies. In fact, our computational results demonstrate for this case the existence of two possible resonance regimes.

One can observe the primary resonance when the modulation period is close to the value T_∞, which can be measured far away from the center of the unperturbed trajectory. As mentioned above [see (12)], this value is equal to the

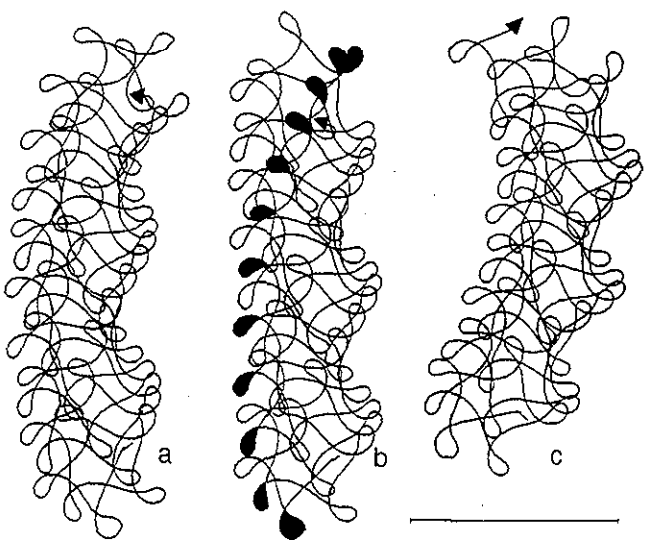

FIG. 3. Resonance drift of the spiral wave (primary resonance) computed for model (3) with $f=2.0$, $\phi_0=0.01$, and modulation amplitude $A=0.0001$. Modulation period: (a) $T_m=3.56$, (b) $T_m=3.57$, and (c) $T_m=3.58$. Scale bar: 10.0. In (b) every fifth lobe of the trajectory is blacked out to indicate a rotation accompanying the drift.

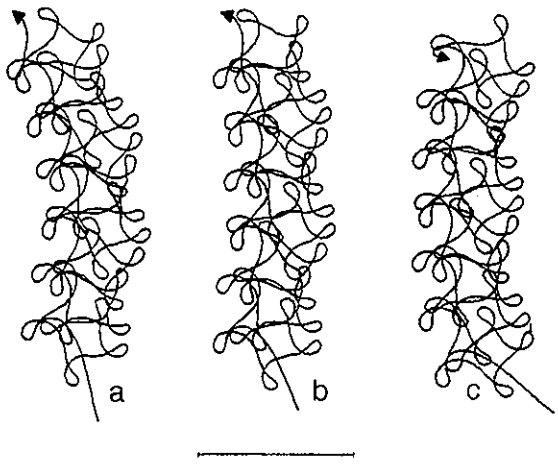

FIG. 4. Resonance drift of the spiral wave (secondary resonance) computed for model (3) with $f=2.0$, $\phi_0=0.01$, and modulation amplitude $A=0.0005$. Modulation period: (a) $T_m=13.0$, (b) $T_m=13.1$, and (c) $T_m=13.3$. Scale bar: 10.0.

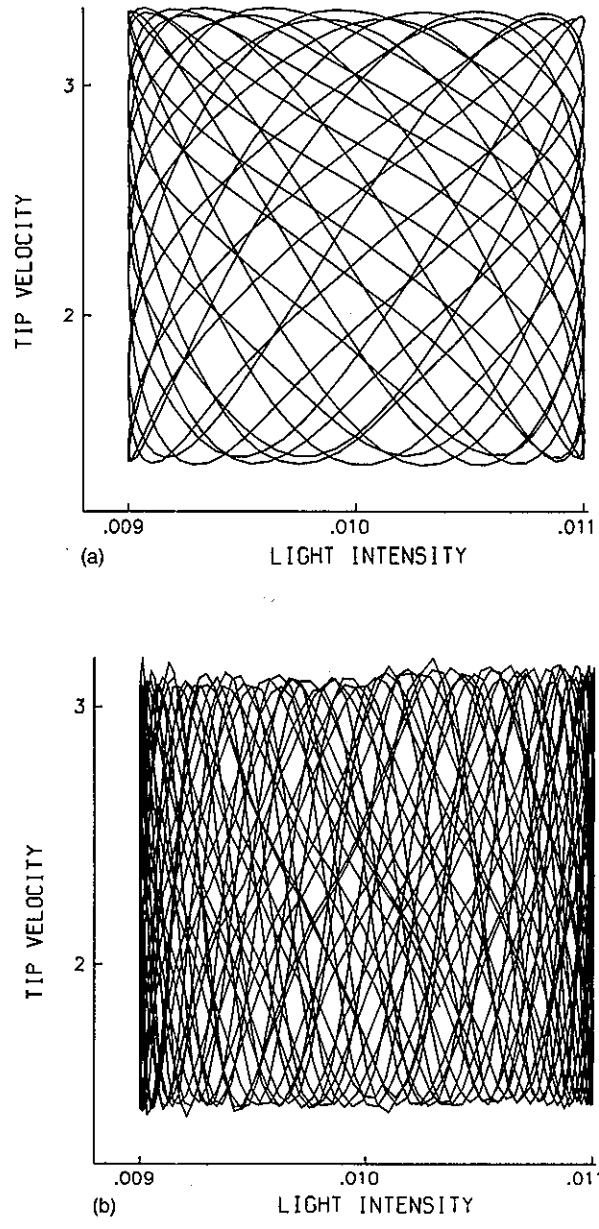

FIG. 5. Variations of the tip velocity with respect to the additional flow of bromide induced by light computed for the case of (a) the primary resonance and (b) the secondary resonance (cf. Figs. 3 and 4, respectively).

period of the primary motion T_1. In Fig. 3, three examples of the tip trajectories are shown that were computed for the model (3), with external forcing with periods close to T_1. The corresponding unperturbed trajectory is presented in Fig. 2(b). The maximum and minimum of the additional bromide flow lie inside the range of the constant flows that correspond to the trajectories in Figs. 2(a) and 2(c). Hence, only small variations of the tip trajectory can be expected during one period of the external forcing. But these variations are accumulated with time.

In Fig. 3(b), the phenomenon of a full primary resonance takes place. For $T_m=T_\infty$, the symmetry center of this trajectory moves with time along a practically straight line. For $T_m<T_\infty$ [Fig. 3(a)], the trajectory of the symmetry center is a circle with a radius $R_c<0$, while for $T_m>T_\infty$, it is a circle with a radius $R_c>0$ [Fig. 3(c)]. The velocity of the resonance drift becomes two times smaller when the amplitude of the external influence is reduced to half its value.

Hence, this primary resonance obeys the relationship (4) derived for the case of resonance under conditions of rigid rotation. But the final picture is much more complicated. The unperturbed trajectory is not only shifted with time, but it also rotates. One can follow this rotation by marking every fifth lobe of the trajectory, as is done in Fig. 3(b).

A qualitatively different resonance regime is observed when T_m is close to the period T_2 of the secondary motion along the unperturbed trajectory (see Fig. 4). In this case, the resonance drift along a straight line exists as well [Fig. 4(b)], and its velocity is proportional to the external amplitude. But for $T_m<T_2$, the symmetry center of each five-lobed fragment describes a circle with radius $R_c>0$ [Fig. 4(a)] and for $T_m>T_2$ one has $R_c<0$. Obviously, the secondary resonance cannot be described by the expression (4), but it is necessary to change the sign in this formula.

The reason for this discrepancy is the following: The expression (4) is valid for the rigid counterclockwise rotation. For the clockwise rotation, the sign of R_c in (4) should be changed. The primary resonance is a result of the external influence on every lobe of the meandering spiral. Each individual lobe describes a counterclockwise rotation in our computations. Hence, the formula (4) should be valid for the primary resonance. The secondary resonance presents the result of external forcing with a period close enough to the period of the secondary motion. But this motion proceeds in a clockwise manner, as mentioned above. Therefore, the sign in the formula (4) should be changed to describe the secondary resonance.

As a significant result, both for the primary and the secondary resonances, no synchronization between the phases of tip motion and external forcing is realized. To illustrate this fact, the tip velocity is plotted in Fig. 5 as a function of

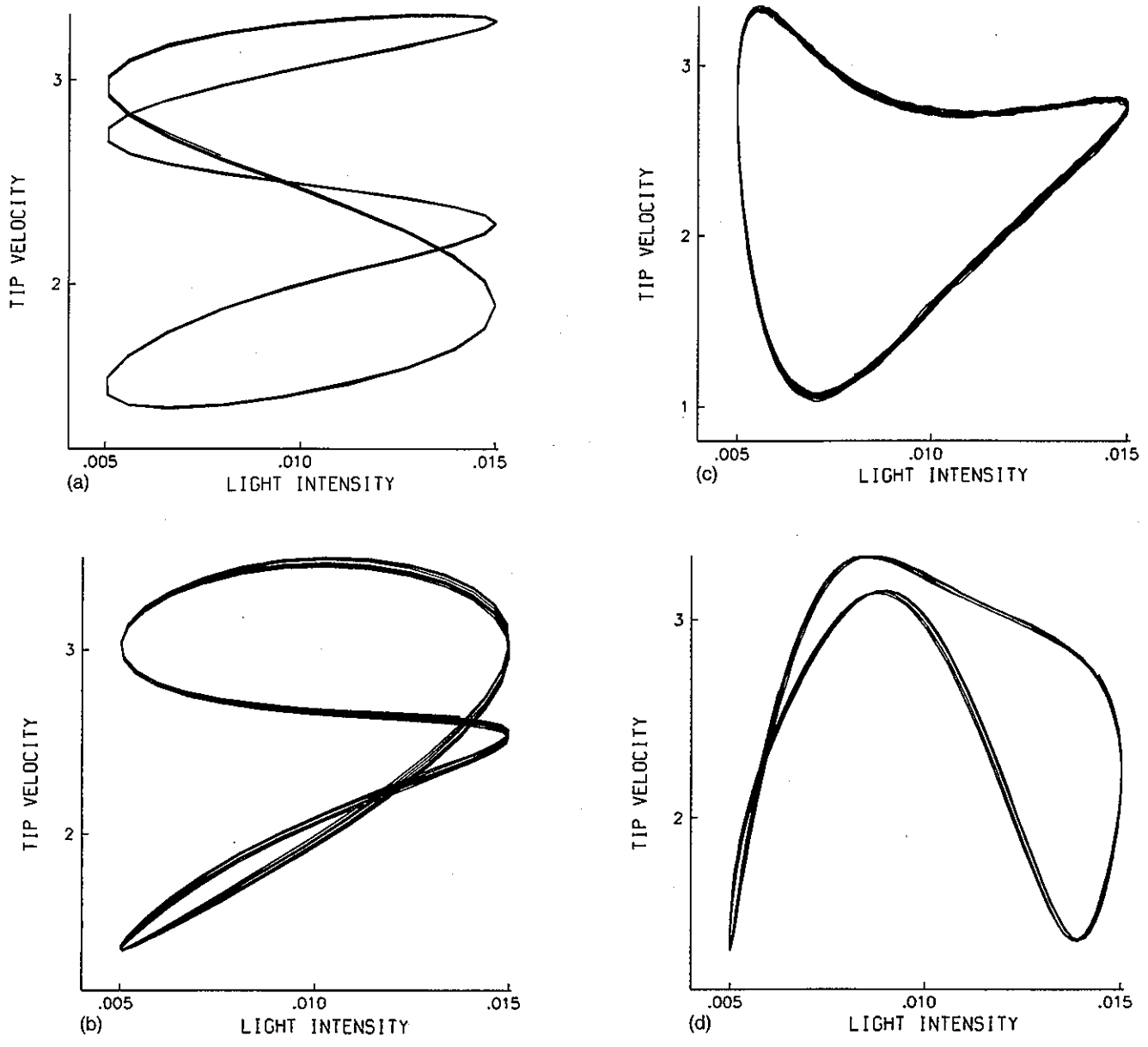

FIG. 6. Variations of the tip velocity with respect to the additional flow of bromide computed for model (3) with $f=2.0$, $\phi_0=0.01$, and modulation amplitude $A=0.005$. The modulation period is: (a) $T_m=0.95$, (b) $T_m=1.4$, (c) $T_m=3.63$, and (d) $T_m=6.0$.

the external intensity. The value of the tip velocity oscillates in time, but the phase of these oscillations is not synchronized by the external forcing. The temporal picture in Fig. 5 looks like a disordered motion, although the spatial motion of both the secondary and primary resonance drift (Figs. 3 and 4) is well ordered.

VI. SYNCHRONIZATION OF SPIRAL WAVES

The phenomenon of synchronization of the spiral wave by external periodical forcing was discovered recently.[30] This effect is illustrated by Fig. 6, in which the spiral tip velocity is plotted as a function of the intensity of external forcing for different values of the modulation period. In several ranges of the modulation period, one can observe phase-locked motion for the given amplitude A of the external signal. In Fig. 6(c), the frequency of the oscillation of the tip velocity is equal to the external frequency. In Fig. 6(a) [resp. Fig. 6(b)], synchronization also occurs, but the tip velocity oscillates with a frequency that is three times (resp., two times) smaller than the external frequency. An example of a synchronization with a frequency two times larger than the external one is shown in Fig. 6(d).

In principle, similar effects are well known for a single nonlinear oscillator.[31,32] But for the spiral wave, such temporal synchronization leads to nontrivial spatial behavior that cannot be reduced to the case of one spatial dimension. Indeed, the synchronization is accompanied by a very strong deformation of the tip trajectory, until even an unrestricted spatial motion occurs.

The main family of trajectories detected in our compu-

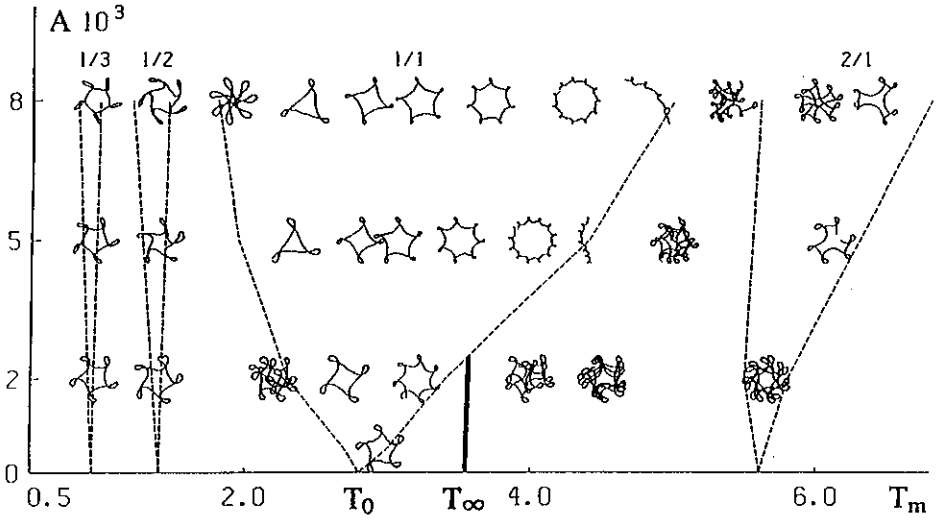

FIG. 7. Tip trajectories computed as a response to sinusoidal modulation of the additional flow of bromide. Trajectories (not to scale) are shown in the plane spanned by the amplitude A and the period T_m of modulation. Dashed lines indicate boundaries of entrainment bands related to different ratios l/m, where l is the number of lobes per m periods of the modulation. Here, T_0 is the intrinsic period of the unperturbed meandering spiral. The thick vertical bar indicates the region of primary resonance.

tations is shown in Fig. 7. The shape of the trajectory depends on both the amplitude A and the period T_m of the external modulation. The dotted lines indicate the boundaries of the so-called Arnold tongues. Inside these tongues the synchronization occurs. Every tongue corresponds to a defined ratio of the number of the lobes per one modulation period.

The broadest tongue (1/1) includes the trajectories with just one lobe per one modulation period [compare Fig. 6(c)]. It is important to point out that the root of this tongue corresponds to the value of the modulation period $T_m=T_0$. As mentioned before, T_0 is the excitation period measured in the symmetry center of the unperturbed hypocyclic trajectory. In the limit of a small modulation amplitude, the synchronization is observed in a very narrow interval of modulation periods around the value T_0. The difference between the trajectory of the synchronized motion, and the unperturbed one is negligible. The width of the synchronization band increases with the modulation amplitude. Simultaneously, the range of deviations in the trajectory increases, as well. For the value $A=0.005$, this leads to practically unrestricted spatial motion near the right boundary of the Arnold tongue (see Fig. 7). The tip trajectory observed for such a parameter set describes many lobes located along a circle with a very large radius. Near the left boundary of the same Arnold tongue, the trajectory is also strongly deformed. But in this case the number of lobes is smaller than for the unperturbed trajectory. Of course, the number of lobes for a hypocycloid cannot be smaller than two. For the amplitude $A>0.005$, the number of lobes observed near the left boundary of the synchronization band is smaller than three and rather close to the theoretical limit. Indeed, for $A=0.005$ we observed a tip trajectory that can be characterized by the lobe number $n=\frac{8}{3}$. Therefore, this hypocyclic trajectory is closed and includes eight lobes, but the trajectory describes three whole rotations around the center. In this sense, the ratio $n=\frac{8}{3}\approx 2.66$ specifies the number of lobes per one rotation around the center. For $A=0.008$ the minimal number of lobes is $n=\frac{7}{3}\approx 2.33$ for the trajectory computed with $T_m=2.0$ (see Fig. 7).

Another Arnold tongue (2/1) includes the trajectories that describe two lobes per one modulation period [compare Fig. 6(d)]. The root of this tongue corresponds to the value $T_m=2\times T_0$. For a very small external amplitude, the deformations of the unperturbed trajectory are, generally speaking, also small. But even a small deformation can result in the appearance of trajectories that look rather exotic. For instance, the trajectory computed for $T_m=5.6$ and $A=0.002$ (see Fig. 7) includes 14 lobes, which are arranged in a perfect symmetric order. For a larger amplitude ($A=0.005$ or $A=0.008$) we observe trajectories in which the lobes are grouped in pairs. These pairs of lobes can be organized in space in a surprisingly complex manner.

In the left part of Fig. 7, two Arnold tongues ($\frac{1}{3}$) and ($\frac{1}{2}$) are shown [compare Figs. 6(a) and 6(b), respectively]. They are not as broad as the two tongues just described and the deformation of the unperturbed trajectory is less pronounced. The roots of these tongues correspond exactly to $T_m=T_0/3$ and $T_m=T_0/2$. In this we find an additional proof that, namely, the value T_0, which is measured in the center of the unperturbed trajectory, determines the observed synchronization processes.

We recall that an external modulation with the period $T_\infty=T_0 n/(n-1)$ results in the primary resonance [Eq. (13)]. In Fig. 7, the resonance zone is shown by a dark solid line. When choosing different amplitudes the primary resonance occurs for almost the same modulation period. Therefore, the resonance zone is practically parallel to the Y axis and intersects the boundary of the Arnold tongue. In the vicinity of

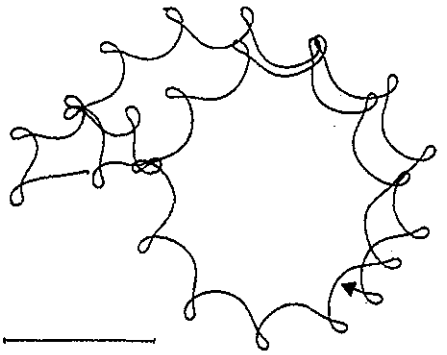

FIG. 8. The tip trajectory computed for the modulation period $T_m=3.63$, which is close to T_∞. The amplitude $A=0.003$ is chosen inside the broadest synchronization band.

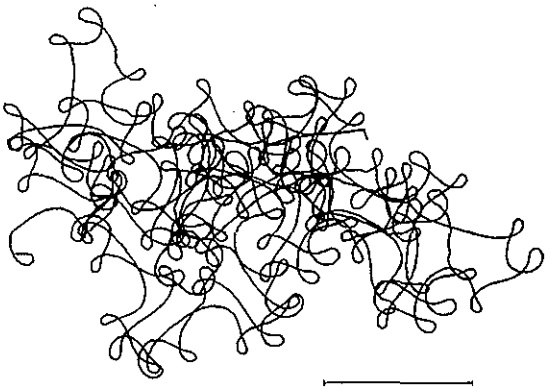

FIG. 10. Irregular tip trajectory computed for model (3) with $f=2.0$, $\phi_0=0.01$, and modulation amplitude $A=0.005$. The modulation period is $T_m=5.4$.

this point of intersection, the resonance regime and the synchronization regime should coexist.

The tip trajectory in this region was investigated in detail and a characteristic example of such a trajectory is shown in Fig. 8. The initial part of the trajectory is very similar to the resonance trajectory (see Fig. 3). The synchronization is absent during the first several lobes, but in the course of time the synchronization becomes effective and the trajectory obtains the shape of a hypocycloid typical for the synchronization band. It appears that the resonance regime is unstable for the parameter region inside the Arnold tongue, whereas the synchronization regime is stable.

VII. IRREGULAR MOTION

Irregular motion is the most probable dynamical regime in an externally forced excitable medium. In fact, any small variations of the parameters of the medium will change both the wave front velocity and the angular velocity of the tip, and thus will disturb the regularity of the unperturbed trajectory. At least two quite different irregular regimes were observed.

The first possibility corresponds to the case when the value of the external period is somewhat too large with respect to T_0, the period at the center. Then one can observe slow variations of the unperturbed trajectory in the range that corresponds to Figs. 9(a) and 9(c). This is certainly an example of an irregular motion, although the variations of the spatial characteristics of the tip motion are not strong. The tip moves in a restricted territory having a similar size as that of the unperturbed trajectory.

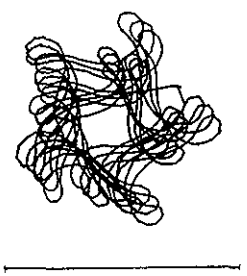

FIG. 9. Irregular tip trajectory computed for model (3) with $f=2.0$, $\phi_0=0.01$, and modulation amplitude $A=0.005$. The modulation period is $T_m=40.0$.

Another type of an irregular motion is observed when the value of the modulation period is about $2\times T_0$. An example of such type of motion is shown in Fig. 10. In this case, the tip describes a highly complex trajectory, and the domain in which this motion occurs becomes very large.

If the modulation period is smaller than $T_0/3$, the external forcing practically does not change the unperturbed trajectory. The variations of the parameters are too fast, and they are simply time averaged.

The trajectories shown in Fig. 7 indicate that the phenomena of synchronization and irregular motion are more general than the resonance effects. Indeed, the thick line in Fig. 7 indicates the domain in the parameter space corresponding to the primary resonance. This domain is very narrow with respect to the considered parameter range of external influence. As a consequence, in the experiments with the BZ reaction, the existence of the phenomenon of synchronization should be examined more easily than the resonance effects.

VIII. EXPERIMENTS

In our experiments we used a photosensitive version of the BZ reaction using $Ru(bpy)_3^{2+}$ as a catalyst.

In the experiments, $Ru(bpy)_3^{2+}$ (4 mM) was immobilized in a silica-gel matrix[33] (thickness 0.7 mm, diameter 7 cm). The reactant concentrations (disregarding bromination of malonic acid) were 0.09 M NaBr, 0.19 M $NaBrO_3$, 0.17 M malonic acid, and 0.35 M H_2SO_4. The temperature was kept fixed at (23±1 °C). White light (halogen lamp, 150 W) illuminating the entire observation area was polarized by a rotating polarization filter and applied to the active medium through a tilted glass plate. Due to polarization, the intensity of the reflected light depends on the orientation of the polarization vector. For the given experimental conditions, the maximum of the light intensity was about 1.36 mW/cm^2, while the minimum was 0.49 mW/cm^2. The two-dimensional

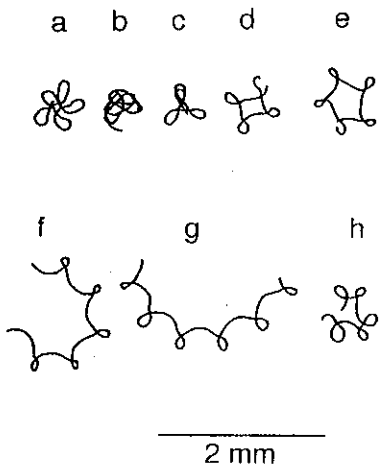

FIG. 11. Sequence of tip trajectories measured in the light-sensitive BZ reaction under sinusoidal modulation of light intensity with amplitude 0.44 mW/cm^2 and period T_m: (a) 17.0, (b) 24.1, (c) 26.2, (d) 29.0, (e) 30.4, (f) 32.9, (g) 34.5, and (h) 52.2 s. Scale bar: 0.2 mm.

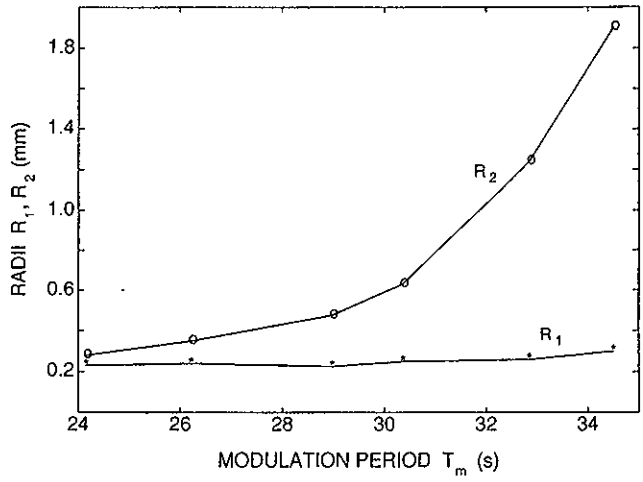

FIG. 12. Radii of the primary and the secondary motion (R_1 and R_2, respectively) as a function of modulation period T_m.

transmission of the medium was detected by a charge-coupled-device camera (Hamamatsu C3077) at 490 nm; stored on a video recorder, and finally digitized by an image-acquisition card.

A spiral wave was created by using a thin laser beam that strongly suppresses the excitability in a small segment of the medium. A propagating circular wave front is broken by collision with such a segment. This creates two open ends of the wave and two spirals rotating in opposite directions are initiated. One of the spirals can be removed by shifting one of the open ends to the boundary of the dish.[18] The temporal trace of the wave tip was detected visually with a reticle in digitized images. The trajectory observed under illumination with an intermediate value of the light intensity of 0.93 mW/cm^2 was an almost five-lobed hypocycloid with a wave period $T_0=24.5$ s at the center of the meandering pattern. Decreasing the stationary level of the illumination down to 0.49 mW/cm^2, or increasing it up to 1.36 mW/cm^2, leads to only relatively small variations of the spatiotemporal behavior of the spiral wave. When applying the minimum and maximum (stationary) intensity, we observed four- and six-lobed trajectories, respectively (similar to Fig. 2).

A rotation of the polarized vector with a constant angular velocity results in a periodical sinusoidal modulation of the illumination. Such periodic forcing induces very strong deformations of the unperturbed trajectory, even though it occurs within the same range of the applied light intensity as for the just mentioned stationary case. In Fig. 11, several characteristic examples of the tip trajectories recorded for different values of the modulation period are shown. This family of trajectory shapes is very similar to the computer results obtained for the amplitude of external forcing $A=0.005$ (see Fig. 7).

The trajectories in Figs. 11(b)–11(g) are the members of one broad synchronization band with one lobe per one external cycle. The trajectory in Fig. 11(h) presents an example of the subsequent synchronization band with two lobes per one external period. In the period range between these two bands, a strongly irregular shape of the trajectory was observed. Figure 11(a) gives an example of the trajectory with one lobe per two external periods.

In order to specify quantitatively the variation of the trajectory shapes with the increase of the modulation period, we used the description of a hypocyclic trajectory given in (5). Each trajectory that belongs to the main entrainment bands was represented by polar coordinates (r,ϕ). The origin of the coordinate system was placed in the symmetry center of the hypocycloid. Two oscillating functions, $r(t)$ and $\phi(t)$, determine the trajectory in a parametric form. The maximum value of $r(t)$, $r_{\max}$, and the minimum one, $r_{\min}$, were estimated and used to determine the radii $R_1=(r_{\max}-r_{\min})/2$ and $R_2=(r_{\max}+r_{\min})/2$. The results of these calculations are presented in Fig. 12 in terms of the functions $R_1(T_m)$ and $R_2(T_m)$.

According to this figure the radius R_1, which characterizes the primary motion, is practically the same for any period of the external modulation. On the other hand, the radius R_2 grows rapidly when the modulation period T_m is increased.

The time interval between the local extrema of the function $r(t)$ determines the period T_0, which can be also measured directly in the center of the trajectory. This period was analyzed for different values of T_m. As shown in Fig. 13, the value T_0 remains practically equal to the value of the external period T_m.

The angular velocity of the secondary motion ω_2 was estimated by determining the average value of $d\phi/dt$ over several periods of the primary motion. The results for the corresponding period $T_2=2\pi/\omega_2$ are shown in Fig. 14. The period T_2 increases rapidly with T_m and appears to be an exponential function of T_m.

Finally, Eq. (10) was used, for estimating the number of lobes n per one rotation period of the secondary motion. On the basis of the data displayed in Figs. 13 and 14, we obtained function $n(T_m)$ that is shown in Fig. 15. Just as the period T_2, the number of lobes n also increases rapidly with

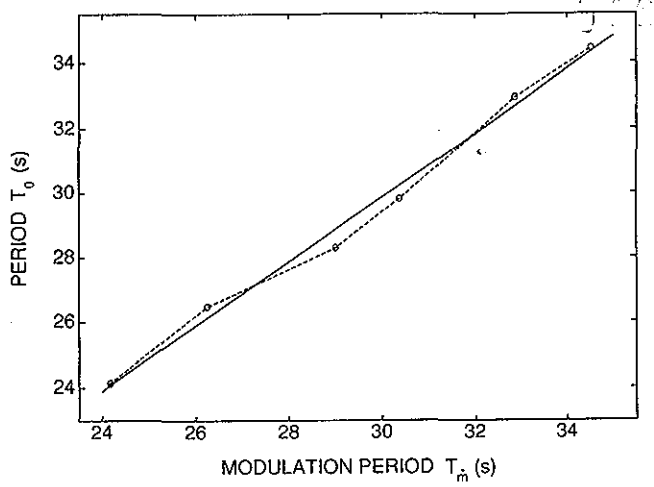

FIG. 13. Period of excitation T_0 measured in the center of a hypocyclic trajectory for different values of modulation period T_m.

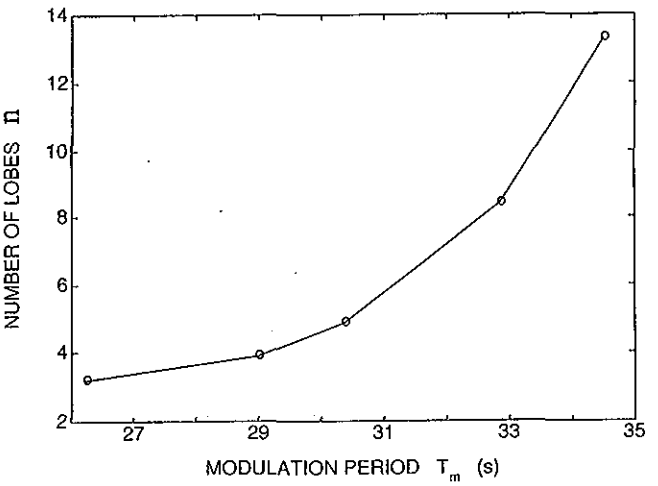

FIG. 15. Number of lobes n estimated by Eq. (10), with the data from Figs. 13 and 14 as a function of modulation period T_m.

T_m. This function describes quantitatively the effect of the deformation of the tip trajectory under external forcing that was presented qualitatively in Fig. 11.

Thus, the deformation of the unperturbed trajectory observed in the experiments is caused mainly by changing the parameters of the secondary motion, R_2 and T_2, whereas the parameters of the primary motion remain practically the same for the different values of the external period T_m. The strong increase of R_2 leads to a pronounced enlargement of the territory of the medium into which the tip is carried by its complex motion.

IX. CONCLUSIONS

A variety of interesting features are observed in the behavior of the spiral waves as a result of external forcing of an excitable medium. The observed effects of resonance, synchronization, period doubling, or irregular motion are very common in nonlinear oscillating systems. It is shown, however, that spiral waves submitted to external forcing exhibit nontrivial dynamic properties and that the resulting spatiotemporal patterns observed in computations and experiments have no direct analogies in the known scenarios of nonlinear oscillators.

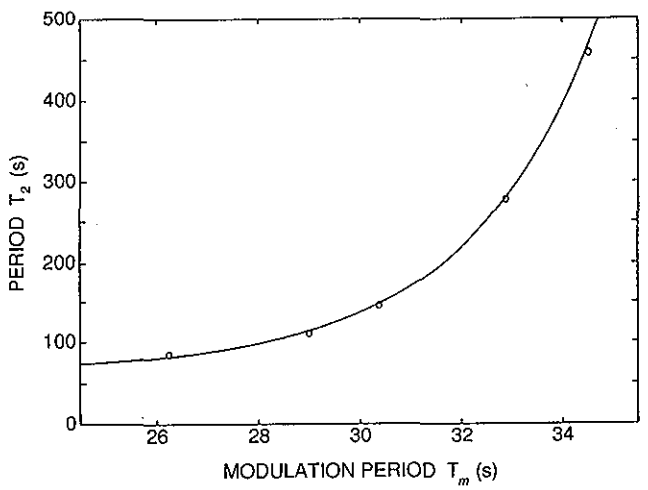

FIG. 14. Period of the secondary motion T_2 estimated from the experimental data as a function of modulation period T_m.

Under external forcing of an active medium there occur simultaneously changes in the propagation velocity, the angular velocity and the curvature of the tip trajectory, the refractoriness, the threshold of excitation, and so on. These values depend not only on time, but differ within the medium. The most probable response of the system in such a situation is an irregular motion of the spiral wave tip (see Figs. 9 and 10). But our computations prove the existence of well-organized regimes: the primary and the secondary resonance and the synchronization of the spiral wave by external forcing.

For the primary and the secondary resonance, the temporal oscillations of the tip velocity are not synchronized by the external forcing, nevertheless, the trajectory is well organized in space. The shape of the unperturbed trajectory is not changed significantly: it is only displaced and rotates with time. For both kinds of resonance, the drift velocity is proportional to the external amplitude. The primary resonance is detected in a very restricted range of the external period, and occurs only for sufficiently small amplitudes (see Fig. 7). If the amplitude is too large, the resonance becomes unstable, and a transfer into the synchronization regime takes place that modifies the tip trajectory drastically.

The synchronization effects are characterized by the existence of Arnold tongues (see Fig. 7). The deformation of the tip trajectory can be very strong, leading to the appearance of an infinite motion of the spiral core. This phenomenon was experimentally observed and studied in the light-sensitive BZ solution. It was shown that the external forcing mainly affects the parameters of the secondary motion of the tip, while the parameters of the primary motion remain practically unchanged.

From a formal point of view, the different kinds of the observed regimes can be explained in terms of variations of

the trajectory curvature. For the rigid rotation the curvature of the tip trajectory is constant. Small periodic variations of the curvature create a cycloidal trajectory and the resonance drift. If the unperturbed trajectory is a cycloid, the curvature is an oscillating function of time and the external forcing can synchronize this nonlinear oscillator. A mechanism for the synchronization is a problem currently under consideration. But such a general kinematical description of the spiral wave dynamics proves that the effects of the synchronization and the resonance are very common for excitable media that should result from different kinds of external forcing. Thus, the external forcing is very useful to study the dynamical features of excitable media and is an efficient means to control spiral wave behavior.

ACKNOWLEDGMENT

V.S.Z. acknowledges support from the WE-Heraeus-Stiftung, Hanau.

[1] M. A. Allesie, F. I. M. Bonke, and F. J. G. Schopman, Circ. Res. **41**, 9–18 (1973).
[2] J. M. Davidenko, A. V. Pertsov, R. Salomonsz, W. Baxter, and J. Jalife, Nature **355**, 349–351 (1992).
[3] N. Gorelova and J. Bures, J. Neurobiol. **14**, 353–363 (1983).
[4] G. Gerisch, Naturwiss. **58**, 430–438 (1971).
[5] J. Lechleiter, S. Girard, E. Peralta, and D. Clapman, Science **252**, 123–126 (1991).
[6] A. T. Winfree, Science **175**, 634 (1972).
[7] R. J. Field and M. Burger, in *Oscillations and Traveling Waves in Chemical Systems* (Wiley, New York, 1985).
[8] S. Jakubith, H. H. Rotermund, W. Engel, A. von Oertzen, and G. Ertl, Phys. Rev. Lett. **65**, 3013–3016 (1990).
[9] S. C. Müller, Th. Plesser, and B. Hess, Physica D **24**, 71–86 (1987).
[10] W. Jahnke, W. E. Skaggs, and A. T. Winfree, J. Phys. Chem. **93**, 740–749 (1989).
[11] Th. Plesser, S. C. Müller, and B. Hess, J. Phys. Chem. **94**, 7501–7507 (1990).
[12] G. S. Skinner and H. L. Swinney, Physica D **48**, 1–16 (1991).
[13] W. Jahnke and A. T. Winfree, Int. J. Bifurcation Chaos **1**, 445–466 (1991).
[14] Zs. Nagy-Ungvarai, J. Ungvarai, and S. C. Müller, Chaos **3**, 15–19 (1993).
[15] V. I. Krinsky and K. I. Agladze, Physica D **8**, 50–56 (1983).
[16] K. I. Agladze, V. A. Davydov, and A. S. Mikhailov, JETP Lett. **45**, 767–770 (1987).
[17] J. Schütze, O. Steinbock, and S. C. Müller, Nature **356**, 45–47 (1992).
[18] O. Steinbock and S. C. Müller, Physica A **188**, 61–67 (1992).
[19] O. Steinbock and S. C. Müller, Int. J. Bifurcation Chaos **3**, 437–443 (1993).
[20] M. Braune and H. Engel, Chem. Phys. Lett. **211**, 534–540 (1993).
[21] R. J. Field, E. Körös, and R. M. Noyes, J. Am. Chem. Soc. **94**, 8649–8664 (1972).
[22] J. J. Tyson, in *Oscillations and Travelling Waves in Chemical Systems*, edited by R. Field and M. Burger (Wiley, New York, 1985), pp. 93–144.
[23] L. Kuhnert, Naturwiss. **73**, 96–97 (1986).
[24] H.-J. Krug, L. Pohlmann, and L. Kuhnert, J. Phys. Chem. **94**, 4862–4866 (1990).
[25] V. S. Zykov, *Simulation of Wave Processes in Excitable Media* (Manchester University Press, Manchester, 1988).
[26] V. A. Davydov, V. S. Zykov, and A. S. Mikhailov, Sov. Phys. Usp. **34**, 665–684 (1991).
[27] V. S. Zykov, Biofiz. **31**, 862–865 (1986).
[28] A. T. Winfree, Chaos **1**, 303–334 (1991).
[29] D. Barkley, M. Kness, and L. S. Tuckerman, Phys. Rev. A **42**, 2489–2492 (1990).
[30] O. Steinbock, V. S. Zykov, and S. C. Müller, Nature **366**, 322–324 (1993).
[31] A. V. Holden, M. Markus, and H. G. Othmer, in *Nonlinear Wave Processes in Excitable Media* (Plenum, New York, 1991).
[32] H. G. Schuster, *Deterministic Chaos* (VCH, Weinheim, 1989).
[33] T. Yamaguchi, L. Kuhnert, Zs. Nagy-Ungvarai, S. C. Müller, and B. Hess, J. Phys. Chem. **95**, 5831–5837 (1991).